Defence Research and Development Canada
Recherche et développement pour la défense Canada

The Characterization of an Inexpensive Nodding Laser

Using a 2-D Laser for Scanning Terrain in 3 Dimensions

G. Broten and J. Collier
DRDC Suffield

Technical Report
DRDC Suffield TR 2005-232
December 2005

Canada

The Characterization of an Inexpensive Nodding Laser

Using a 2-D Laser for Scanning Terrain in 3 Dimensions

G. Broten and J. Collier
DRDC Suffield

Defence R&D Canada – Suffield

Technical Report

DRDC Suffield TR 2005-232

December 2005

Author

G. Broten

Approved by

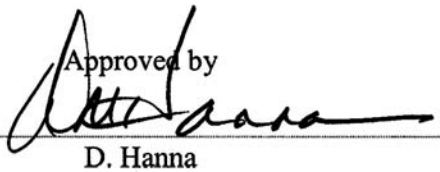

D. Hanna

Head, Autonomous Intelligent Systems Section

Approved for release by

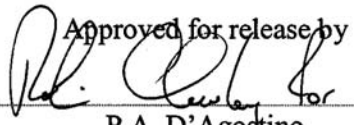

P.A. D'Agostino

Chair, Document Review Panel

Abstract

The accuracy and reliability of laser rangefinders make them a ubiquitous sensing device employed on many unmanned ground vehicles. Expensive, high performance 3-D laser rangefinders enjoy limited acceptance, whereas static mounts are the preferred configuration for low cost 2-D laser rangefinders. This paper investigates and characterizes the factors affecting the nodding 2-D laser's performance. This research determined errors in measuring the vehicle's roll, pitch and yaw have the greatest impact on measurement accuracy. Analysis and simulations revealed that adaptive nodding rates offered unique advantages, especially when used with a terrain map world representation. The nodding mechanism also allows for the acquisition of multiple range data sets over the same terrain patch. These multiple data sets alleviate some of the problems traditionally associated with laser rangefinders, but they place more stringent requirements on the vehicle's pose accuracy. DRDC, in conjunction with Scientific Instrumentation Ltd., developed an inexpensive nodding SICK laser device and this device's 3-D data was an essential contributor to the successful Autonomous Land Systems demonstration.

Résumé

Les télémètres laser sont des appareils très répandus que l'on emploie sur beaucoup de véhicules terrestres sans pilote du fait de leur précision et fiabilité. Les télémètres laser 3-D très performants mais coûteux sont moins acceptés alors qu'on préfère les montages statiques des configurations pour les télémètres laser 2-D qui sont peu coûteux. Cet article étudie et caractérise les facteurs qui affectent le rendement du laser 2-D basculant. La recherche a déterminé que ce sont les erreurs de mesures du roulis du véhicule, du tangage et lacet qui affectent le plus l'exactitude des mesures. Des analyses et des simulations ont révélé que les déplacements angulaires de basculage adaptés offrent des avantages uniques, surtout quand ils sont utilisés avec une représentation du monde réel sous forme de carte morphographique. Le mécanisme de basculage permet aussi l'acquisition d'ensembles de données multiples de distances sur la même parcelle de terrain. Ces ensembles de données multiples atténuent certains problèmes qui étaient traditionnellement associés aux télémètres laser mais ils sont plus exigeants en matière d'exactitude de pose du véhicule. RDDC, avec le concours de Scientific Instrumentation Ltd., a mis au point un appareil laser SICK basculant qui est économique et dont les données 3-D ont contribué de manière essentielle au succès de la démonstration des Systèmes terrestres autonomes.

This page intentionally left blank.

Executive summary

Background: Unmanned Ground Vehicle (UGV) Research and Development within the Autonomous Land Systems (ALS) project will assist the Canadian Forces (CF) in fulfilling their future mandate. DRDC's Technology Investment Strategy defines an Autonomous Intelligent Systems as "...automated or robotic systems that operate and interact in the complex unstructured environments of the future battlespace". Sensing, the first stage in understanding one's environment, is a core requirement and prerequisite to autonomous intelligence.

Autonomous unmanned vehicles (UxVs) must have an adequate world representation in order to safely avoid obstacles and hazards during maneuvers. The most common perception sensor is the reliable and accurate laser rangefinder (LRF). Traditionally found on a fixed mount, the 2-D LRF scans a single terrain slice, thus requiring motion to create a 3-D representation. 3-D LRFs supply multi-scan, 3-D capabilities, but are expensive. This report investigates and characterizes factors affecting 3-D measurements using an inexpensive nodding 2-D LRF.

Principle Conclusions: DRDC and Scientific Instrumentation Ltd. developed a nodding system for the inexpensive SICK LRF. This device allows multiple terrain scans, thus alleviating the occlusion, mixed pixel and sunlight blinding issues associated with the single scan configuration. Integrating multiple terrain scans into a single world representation has numerous advantages, but it also requires an accurate vehicle pose estimation. This work investigated the error sources limiting the accuracy of a vehicle mounted LRF and determined that errors in roll, pitch and yaw were an order of magnitude more significant than any other error source. These errors, when converted to a spherical positional error, can have magnitudes up to 3.0 m. Such a large error, nearly the size of the Raptor unmanned ground vehicle (UGV), cannot be safely ignored. The nodding LRF also enables uniform distance sampling that results in more consistent and accurate world representations.

Significance of Results: DRDC mounted a nodding SICK LRF on the Raptor UGV where it was the primary perception sensor for the Autonomous Land Systems demonstration. Due to time and manpower constraints, the nodding SICK LRF operated at a constant rotational rate. Although the 3-D data produced by this configuration was not as desirable as the uniform distance sampling profile, it was more than sufficient for the Raptor UGV's world representation. Using this world representation, the Raptor UGV navigated between the start and end points, while successfully avoiding obstacles and hazards.

Future Results: For the ALS demonstration, the nodding SICK laser rotated at a fixed rate. Although this initial configuration was sufficient, future work will implement adaptive nodding rates, with uniform sample distance capabilities. A uniform sample distance enables a more accurate world representation since the laser samples the terrain at near equal spacings. This will allow the extremities of the world representation to be nearly as accurate and reliable as the central areas of the world representation.

G.S. Broten and J.A. Collier. 2005. The Characterization of an Inexpensive Nodding Laser. DRDC Suffield TR 2005-232. Defence R&D Canada – Suffield.

Sommaire

Contexte : La recherche et développement des Véhicules terrestres sans pilote au sein du projet des Systèmes terrestres autonomes soutiendra les Forces canadiennes (FC) à remplir leur mandat futur. La Stratégie d'investissement technologique de RDDC définit les Systèmes intelligents autonomes comme « des systèmes robotisés et automatisés qui opèrent et interagissent dans les milieux non structurés des futurs champs de bataille ». La détection qui est la première étape pour comprendre un milieu est un besoin essentiel et une condition préalable à l'intelligence autonome.

Les véhicules autonomes sans pilote doivent posséder une représentation du monde réel adéquate pour éviter les obstacles et les dangers en toute sécurité durant les manœuvres. Le capteur de perception le plus commun est le télémètre laser (LRF) qui est fiable et précis. Traditionnellement sur un montage fixe, le LRF 2-D balaie une seule tranche de terrain, exigeant ainsi une motion pour créer une représentation 3-D. Les LRF 3-D effectuent des balayages multiples ayant des capacités 3-D mais ils sont coûteux. Ce rapport étudie et caractérise les facteurs affectant les mesures 3-D qui utilisent des LRF 2-D basculants qui sont plus économiques.

Conclusions principales : RDDC et Scientific Instrumentation Ltd.ont mis au point un système basculant pour le LRF SICK qui est économique. Cet appareil permet des balayages multiples de terrain ce qui atténue les problèmes d'occlusion, de pixel mixte et d'aveuglement par la lumière du soleil associés avec la configuration pour un seul balayage. L'intégration de balayages multiples de terrain en une seule représentation du monde réel possède de nombreux avantages mais elle exige aussi une estimation précise de la pose du véhicule. Ces travaux ont étudié les sources d'erreur qui limitent la précision d'un LRF monté sur véhicule et ont déterminé que les erreurs de roulis, tangage et lacet étaient d'un ordre de grandeur plus important que n'importe quelle autre source d'erreurs. Ces erreurs, une fois converties en erreurs planimétriques sphériques peuvent avoir des grandeurs allant jusqu'à 3.0 m. Une erreur aussi importante, étant presque de la taille du véhicule terrestre sans pilote Raptor, ne peut pas être ignorée sans danger. Le LRF basculant permet aussi d'échantillonner à des distances uniformes ce qui produit des représentations du monde réel plus stables et plus précises.

La portée des résultats : RDDC a monté le LRF SICK basculant sur le véhicule terrestre sans pilote Raptor sur lequel il était le capteur de perception primaire durant la démonstration des Systèmes terrestres autonomes. À cause des restrictions de temps et de main-d'œuvre, le LRF SICK basculant opérait à une vitesse de rotation constante. Bien que les données 3-D produites par cette configuration n'aient pas été aussi désirables que le profil de l'échantillonnage à une distance uniforme, elles étaient plus que suffisantes pour la représentation du monde réel du Raptor. Le Raptor qui utilisait cette représentation du monde réel naviguait entre les points de départ et d'arrivée tout en évitant les obstacles et les dangers.

Résultats futurs : Durant la démonstration des Systèmes terrestres autonomes, le laser SICK basculant faisait une rotation à une vitesse angulaire fixe. La configuration initiale était suffisante mais les travaux futurs implémenteront des vitesses angulaires adaptées de basculage ayant des capacités d'échantillonnage de distance uniforme. Un échantillonnage d'une distance uniforme permet une représentation du monde réel plus précise puisque le laser échantillonne le terrain à des espaces quasiment égaux. Ceci permettra aux extrémités de la représentation du monde réel d'être aussi précises et fiables que les zones centrales de représentation du monde réel.

G.S. Broten and J.A. Collier. 2005. The Characterization of an Inexpensive Nodding Laser. DRDC Suffield TR 2005-232. R & D pour la défense Canada – Suffield.

Table of contents

List of figures

List of tables

This page intentionally left blank.

1. Introduction

In order to achieve autonomous, high speed, continuous motion navigation over rough, unstructured outdoor environments, an UxV must quickly create an adequate local representation of its world. This local representation extends as far as the sensing limits and allows an obstacle avoidance algorithm to navigate local obstacles[1] that do not appear in global, maps. Creating such a local representation, for a robot with a forward velocity in excess of 2 to 3 m/s, is a challenging problem due to sensing and computational limitations. The most common form for an outdoor world representation, the terrain map[2] [1, 2, 3, 4, 5, 6, 7], requires the world be sensed in three dimensions. Active and passive range sensors have been extensively investigated and used for this purpose. Herbert [8] surveyed range sensing technologies including laser rangefinders (LRF), triangulation rangefinders and passive stereo vision. This report focuses on laser rangefinders because of their reliability and accuracy. Laser rangefinders are available in two configurations, those that directly scan the world in 3 dimensions, and those that scan in 2 dimensions. The high cost of 3-D LRFs have limited their acceptance and usage on UxV's, whereas the low cost 2-D LRF is commonly found on static mounts. Although statically mounted 2-D LRFs will suffice, a nodding LRF configuration offers advantages. A nodding LRF can profile the terrain without the need for vehicle motion and it allows for the acquisition of multiple range data sets over the same terrain. This report investigates a nodding 2-D laser rangefinder configuration and characterizes the factors affecting its performance.

The report consists of 8 sections. Section 2. gives background material on laser ranging devices, and Section 3. provides specific detail on the nodding laser device used in this research. Section 4. investigates nodding profiles and the effects of motion are presented in Section 5. The performance of the nodding SICK laser is detailed in Section 6.. Section 7. summarizes the nodding SICK laser's Miro implementation on the Raptor UGV and provides results from the ALS demonstration. The report finishes with the conclusions given in Section 8.

2. Laser Ranging Devices

2.1 Background

Researchers have investigated and characterized the problems associated with LRFs such as: mixed pixels, range/intensity crosstalk, synchronization, localization and range drift [9, 10, 11, 12]. In the late 1980's the Navlab [13] and Ambler [14] platforms used 3-D LRFs to construct terrain maps. The ERIM [15] and Perceptor [9] 3-D LRFs were very expensive, heavy and bulky; thus, they were not suitable for small, and agile robots.

[1] Such as rocks, berms and vehicles.

[2] Terrain maps are also commonly referred to as digital terrain maps , digital elevation maps or $2\frac{1}{2}$D grid maps.

To overcome the cost and size burden imposed by 3-D LRFs, researchers have turned to inexpensive and light weight 2-D LRFs such as the SICK and the Acuity laser rangefinders[3]. Henriksen and Krotkov used a downward looking Acuity LRF to implement a hazard detection algorithm [16]. CMU used a SICK laser, with a fixed look ahead distance of 5m and the motion of the robot, to generate terrain maps of the Antarctic ice surface [17].

All surveyed 3-D LRF and 2-D LRF implementations, with the exception of Ambler, use only a single sample of the range data; thus, a given patch of terrain is scanned only once. With only a single sample of data common LRF problems, such as mixed pixels, range/intensity crosstalk and occluded regions, must be addressed. The approach taken by Ambler combined multiple terrain maps using a feature matching process. The merging of maps into a composite map had the benefits of a) increased resolution for the parts of the terrain maps originally measured at a distance from the vehicle, and b) added information about previously occluded areas [14]. The occluded region issue was directly tackled by Herbert, Kanade and Kweon via the locus technique for modeling rugged terrain [15, 2]. Ye and Borenstien [18] implemented an image processing technique called the Certainty Assisted Spatial filter that identified the corrupted pixels and missing data in a terrain map.

2.2 Motivation

Terrain maps based upon a single sample of range data suffer from mixed pixels and occluded regions. A nodding LRF samples the terrain multiple times before the terrain is traversed. As the vehicle moves forward the terrain patch is viewed from different perspectives as shown in Figure 1.

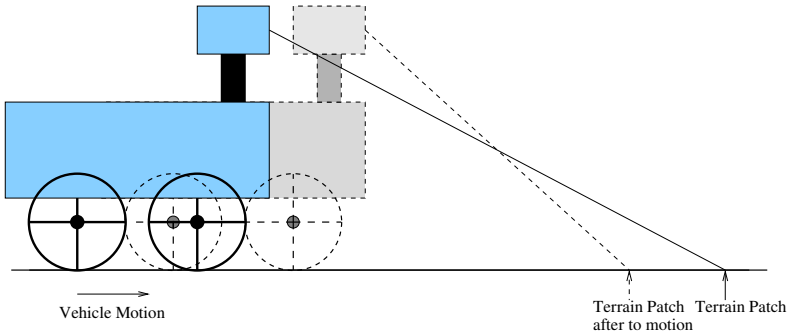

Figure 1: *Perspective change for a terrain patch*

The scanning from multiple perspectives offers the following advantages:

1. Multiple scans reduce the probability of occlusion,

[3]Often referred to as lasers.

2. When viewed from different perspectives, there is a lower probability of encountering a mixed pixel for the same terrain patch,

3. A new perspective on a low diffuse reflectivity region may produce a stronger beam reflection,

4. The LRF could be oriented into a position that is less affected by sunlight.

3. DRDC's Nodding Sick Laser

DRDC, in conjunction with Scientific Instrumentation Ltd., developed a nodding device for the SICK LMS 211 laser. The mechanism consists of a stepper motor with encoder feedback. An embedded controller board handles all data transfers and control of the mechanism. To ensure timeliness, RTEMS, a real-time operating system is used. Other hardware, such as a motor driver board, power supply, and serial interface board, is also integrated into this package. A 10Mbit ethernet interface issues commands and receives data from the scanner. The board downloads its program through an ethernet connection via *tfpt* and *bootp* protocols. Parameters such as nodding rate and sweep angle may be configured at run time. The SICK laser's nodding rate ranges from 2 degrees/sec up to a maximum of 90 degrees/sec. An encoder, with 0.072 degree resolution, provides accurate position feedback. Figure 2 shows the custom nodding mechanism with a SICK laser scanner. The SICK laser determines range by measuring

Figure 2: *Scientific Instrumentation Ltd. Nodding Laser*

the time of flight for a laser light pulse. This process is subject to systematic errors resulting in an accuracy of ± 4 cm when operating in the range of 1 to 30 m. The SICK laser can be configured to return range readings on 1 degree increments over a 180

degree[4] arc. The laser can also operate in the interpolated mode where it returns ranges on $\frac{1}{2}$ degree increments. The angular accuracy of the SICK laser is ± 0.01 degrees.

3.1 Field of View

The nodding SICK laser's field of view (FOV) is defined in a manner analogous to the FOV definition for a camera. The SICK laser's field of view is shown in Figure 3. As can be seen, the SICK laser has a 180 degrees horizontal FOV, and its vertical FOV ranges from $\theta_{start} = 0$ at the horizon, to θ_{end}. By definition angles above the horizon are positive and increasing, whereas angles below the horizon are negative.

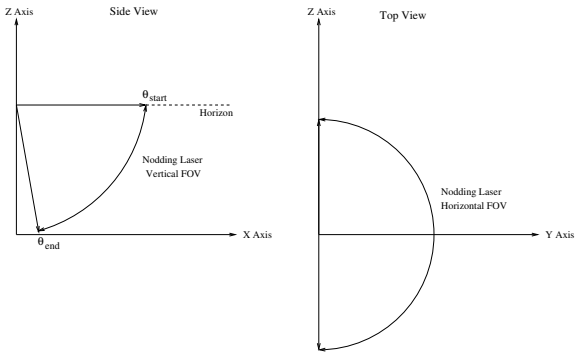

Figure 3: *Nodding SICK Laser FOV*

3.2 Nodding Apparatus

When operating at full data rates the SICK laser completes a scan, corresponding to 180 degree sweep of the laser beam, every 13ms[5]. The nodding mechanism rotates the SICK laser about the Y axis, thus nodding while scanning creates a skewed scan. This skewing process, for the laser nodding away from the ground, is shown in Figure 4.

The encoder is read upon the reception of the last data byte from the SICK laser, as shown in Figure 4. The corrected encoder reading for each range is given by:

$$\theta_c = \theta_r \pm \omega \times \frac{i}{N}$$

where: θ_c is the corrected encoder reading, θ_r is the encoder value read, ω is the angular rotation rate of the nodding device, i is the index into the range data array returned from the SICK laser, and N is the number of range samples.

[4]Corresponding to 181 measured range values.

[5]For the interpolated mode the scan frequency is 26.6ms.

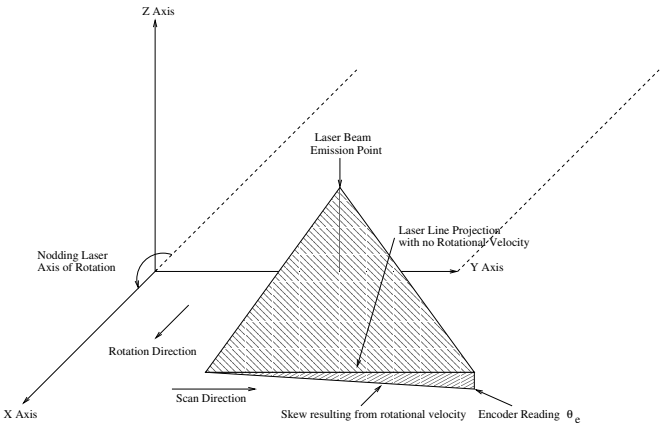

Figure 4: *Skew Resulting from Rotational Velocity*

The nodding rotational direction determines the sign of the correction: positive for an increasing encoder and negative for a decreasing encoder[6].

4. Nodding Profiles

A LRF, mounted on a nodding device, sweeps the terrain in front of the vehicle without requiring the vehicle to move. This nodding action is shown in Figure 5. The position of the laser beam is given by $\theta = \tau \times \omega$ where:

τ = SICK laser sweep period

ω = Angular rotational rate of the nodding device

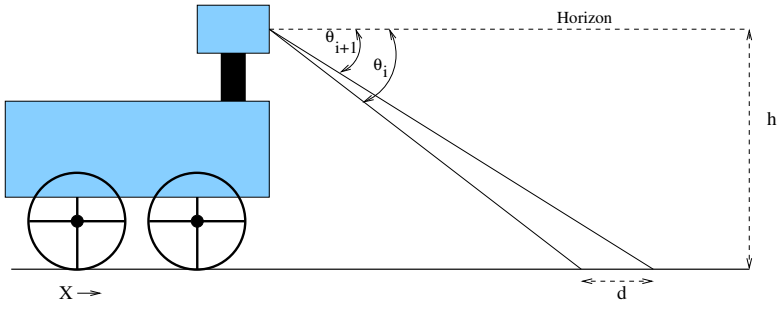

Figure 5: *Sweep of the Nodding Device*

The term sample distance denotes distance along the X axis direction that is covered between successive sweep periods of the LRF and is denoted by d. A sequence of

[6]The encoder on the nodding device is configured such that 0 degrees corresponds to the horizon, with positive angles measured above the horizon and negative angle measured below the horizon.

sample distances is called the nodding profile. The following Sections detail two common nodding profiles.

4.1 Constant angular rotation rate

A constant rotational rate, ω, is the simplest nodding profile. This causes the laser beam to sweep ever larger sample distances as the nodding angle approaches the horizon. The sample distance is given by:

$$d_i = \frac{h}{\tan(\theta_i)} - \frac{h}{\tan(\theta_{i+1})} = \frac{h}{\tan(\omega \times \tau_i)} - \frac{h}{\tan(\omega \times \tau_{i+1})}$$

The sample distance profile resulting from a nodding LRF mounted at a height of 1m, with an angular rotation rate of 30 degrees/s, 60 degrees/s and 90 degrees/s are shown in the following Figures. Figure 6 shows the sample distance versus the rotation angle for angles between 2 and 15 degrees, and Figure 7 shows the results for angles between 15 and 90 degrees.

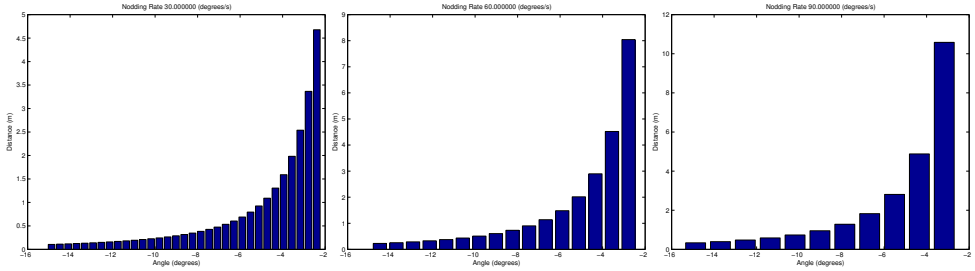

Figure 6: *Sample Distance vs. Rotation Angle, 2-15 Degrees, H=1 m*

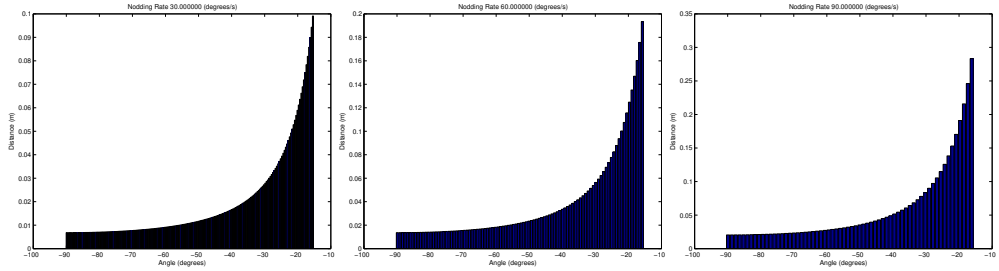

Figure 7: *Sample Distance vs. Rotation Angle, 15-90 Degrees H=1 m*

Figure 8 shows the sample distance profile, over the range of 2 to 15 degrees, resulting from the laser mounted at a 2 m height. Figure 9 show the sample distance for rotational angles between 15 and 90 degrees.

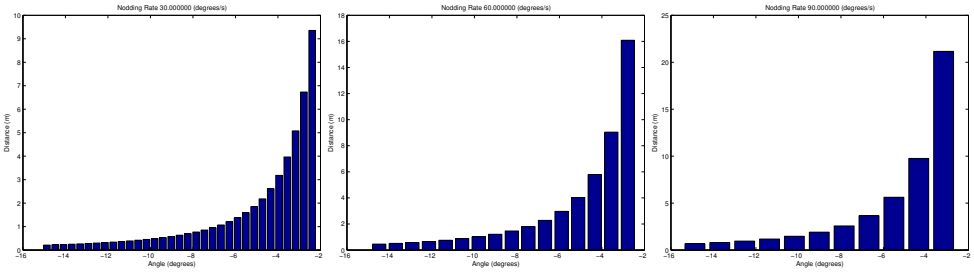

Figure 8: *Sample Distance vs. Rotation Angle, 2-15 Degrees H= 2m*

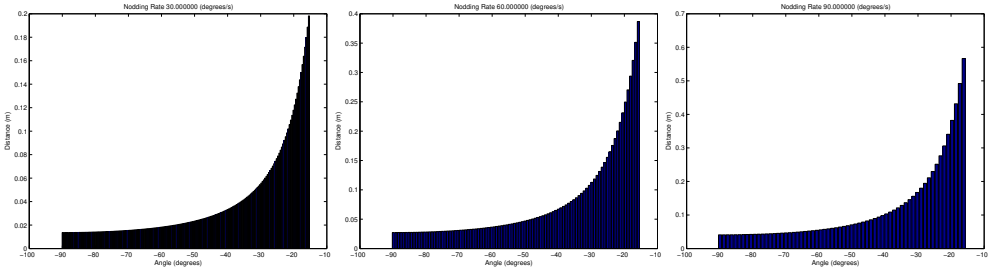

Figure 9: *Sample Distance vs. Rotation Angle, 15-90 Degrees H= 2m*

4.1.1 Discussion

The constant angular rate profile results in highly non-linear sample distances. This profile yields a dense sampling close to the vehicle, and the distant terrain is sparsely sampled. This results in a strong statistical basis towards the nearby terrain. The locus technique for modeling rugged terrain [15, 2] uses a mathematical technique to transform the range data into a uniform sample distance format and thus a data format that more amenable to generating world representations.

4.2 Uniform sample distance

The uniform sample distance profile attempts to maintain a constant sample distance over all nodding angles[7]. The equation governing a uniform sample distance is given by:

$$\theta_{i+1} = \arctan\left(\frac{h \times \tan(\theta_i)}{h - d \times \tan(\theta_i)}\right) = \arctan\left(\frac{h \times \tan(\omega \times \tau_i)}{h - d \times \tan(\omega \times \tau_i)}\right)$$

Figure 10 shows results of an ideal 0.02m uniform sample distance. An adaptive nodding profile must be implementation to achieve the uniform sample distance. The

[7] Within the mechanical capabilities of the nodding device.

relationship between nodding angle and the required rotational rate is show in Figure 10. Unfortunately the ideal uniform sample distance requires a high angular position accuracy and large rotational rates.

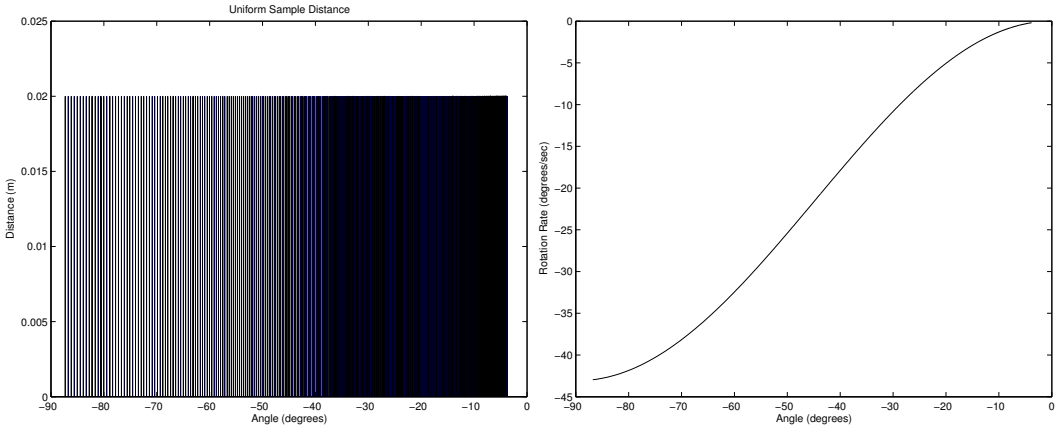

Figure 10: *Uniform Scan Density*

All nodding mechanisms have a finite capability to resolve their angular position. Figure 11 shows the resulting sample distances for a nodding mechanism with a minimum angular resolution of 0.072 degrees and a maximum angular rotation rate of 90 degrees/second. Concluding, the physical characteristics of the nodding device impose accuracy limits. At angles less than 15 degrees and at angle greater that 75 degrees it is no longer possible to maintain an ideal uniform sample distance.

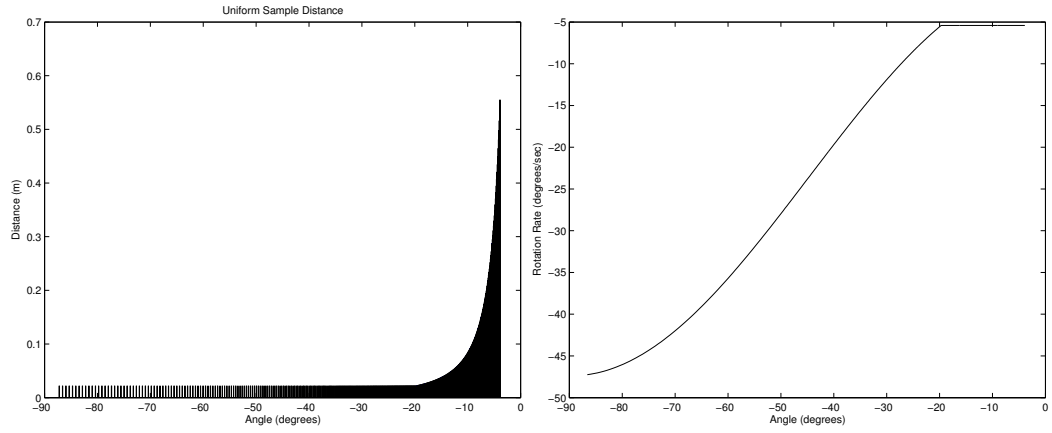

Figure 11: *Uniform Sample Distance*

4.2.1 Discussion

This approach alleviates the near vehicle, statistical basis problem associated with the constant angular rotation rate profile, without requiring a

mathematical transformation such as the locus technique. The uniform sample distance profile produces range data tailored for world representations.

5. Vehicle Motion

The previous sections derived the equations governing a nodding LRF assuming the vehicle is static. Although it is possible to implement a stop and scan behavior, this implementation is not practical for real world situations. Thus, the LRF must operate while the vehicle is in motion. This section modifies the equations developed in the previous sections to include motion. Figure 12 shows the effect of movement on the nodding LRF.

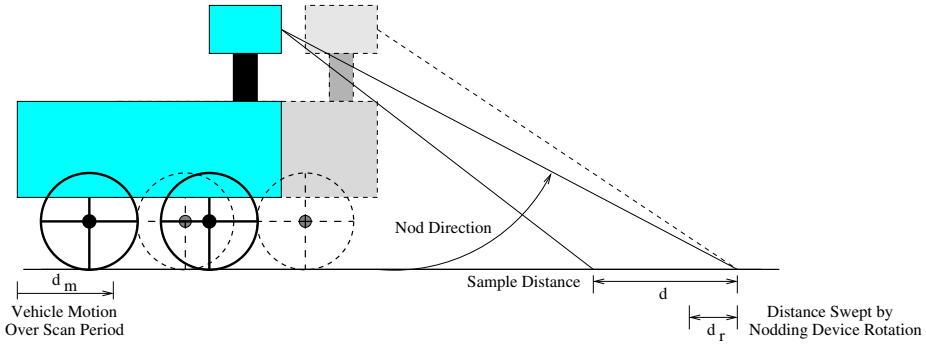

Figure 12: *Uniform Sample Distance with Motion*

Where: d is the desired sample distance, $d_m$is the distance traveled by UGV over the scan period of the LRF and is given by $d_m = v_m \times \tau$. v_m denoted the the vehicle's velocity and τ is laser's scan period.

To maintain a uniform sample distance the nodding mechanism must adaptively compensate for the vehicle's motion, d_m. When the laser nods upward the distance d_m contributes to the distance the laser must cover due to rotation, and for the downwards nodding direction $d_m$works against the nodding device. This process in shown by the following equation:

$$d_r = d \pm d_m = d \pm v_m \times \tau$$

The rotational direction of the nodding mechanism determines the sign used in the above equation. Figure 12 shows the case where the nodding device is traveling from a down looking stance toward the horizon[8] where the vehicle's motion contributes to the sample distance. For this situation the sign is negative. When the nodding device is

[8]Called upwards rotation.

rotating from the horizon towards a down looking stance[9] the motion of the vehicle's motion works against nodding devices travel. Thus, the sign in the above equation is positive. Both of these cases are shown in Figure 13.

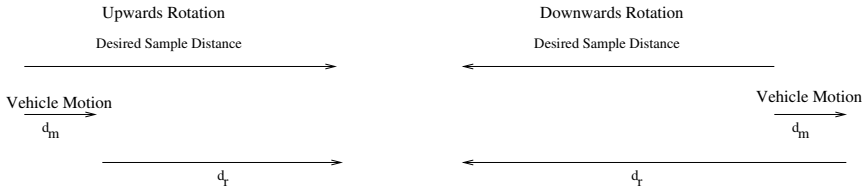

Figure 13: *Vehicle motion relative to Uniform Sample Distance*

5.1 Creating a Uniform Sample Distance with Vehicle Motion

Creating a uniform sample distance, while the vehicle is in motion, requires the nodding mechanism compensate for the movement of the vehicle. The equation governing the uniform sample distance profile, for a stationary platform, was derived in Section 4. and is given by:

$$\theta_{i+1} = \arctan\left(\frac{h \times \tan(\theta_i)}{h - d_r \times \tan(\theta_i)}\right)$$

When the vehicle is in motion the required sample distance is given by:

$$d_r = d \pm v_m \times \tau$$

Thus combining the two equations results in an equation, that compensates for vehicle velocity, to create a uniform sample density.

$$\theta_{i+1} = \arctan\left(\frac{h \times \tan(\theta_i)}{h - (d \pm v_m) \times \tau \times \tan(\theta_i)}\right)$$

The sign of the distance term is determined by the direction of rotation for the nodding device, a subtraction for upwards rotation and an addition for downwards rotation.

5.2 Scanning Dead Zone

A vehicle in motion requires a finite distance to stop[10], thus there is no need to scan the region where an obstacle can not be avoided. This region is called the "dead zone". As

[9] Called downwards rotation.

[10] This is simplistic view, since a swerving motion could allow a vehicle to avoid an obstacle, not to mention the utility of slowing down before hitting an obstacle.

a rough estimate, the reaction and stopping distance is proportional to the velocity of the vehicle and is given by $s \propto v$. Thus the LRF's vertical FOV, as defined in Section 3.1, can be limited by the angle given by:

$$\theta_{end} = 90 - \arctan(\frac{s}{h})$$

where s is the vehicle stopping distance and h is height at which the LRF is mounted.

5.3 Scanning with Vehicle Motion

Assume the target point is at the maximum range of the LRF (30 m), the nodding device must rotate the LRF from its minimum angle of rotation, to its maximum angle of rotation and then back towards the target point before it can be scanned again. The minimum angle is given by the "dead zone", and the horizon defines maximum angle. Matlab simulated a nodding LRF scanning a uniform sample distance. The simulation mounted the LRF 2.0m above the ground, set the vehicle's forward velocity at 2.0 m/s and nodded the LRF in an adaptive manner while attempting to maintain a uniform sample density of 0.20 m[11]. As the vehicle moved forward, the simulation tracked a target point in front of the vehicle until the target exited the FOV. Thus, the combined effects of vehicle motion and LRF nodding were investigated.

Figure 14 shows the distance between the LRF scan and the target point as a function of time. As can be seen, the target point is scanned a total of 8 times.

5.3.1 Minimum Distance to Target

Due to the LRF's slow sweep period and the motion of the vehicle, the LRF[12] usually does not scan the exact target point, but instead scans in the near vicinity of the target point. Figure 15 shows the minimum distance between the LRF scan and the target point, each time the LRF passed within the vicinity of the target point. The figure shows the target point region was scanned 8 times and this value is called the frequency of scan. As expected, the LRF scans nearer the target point when the nodding device is at larger angles of rotation below the horizon. This condition occurs as the vehicle's forward movement brings it near the target point. These minimum distances to the target can be summed and divided by the number of passes to determine the mean distance to the target. This mean distance to the target is used as the measure of the system's fidelity.

[11] The physical limitation of the nodding device, including the encoder resolution and maximum angular rotation rates, were modeled in the simulation.

[12] This simulation had a LRF sweep period of 13.3 ms.

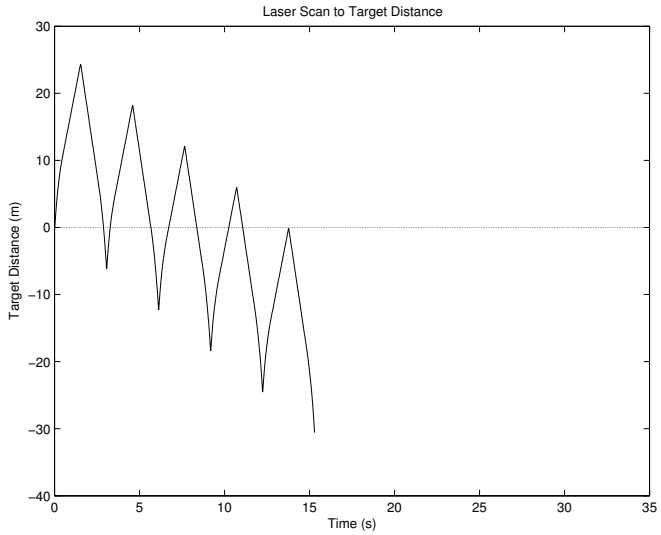

Figure 14: *LRF Scan to Target Distance*

5.3.2 Velocity and Sample Distance Relationship

A simulation was used to investigate the relationship between the nodding device's rotational rates and the forward velocity of the vehicle. It was determine the sample distance and the frequency of scan are opposing factors. A smaller sample distance yields a finer resolution, but requires a slower nodding rate. The slower rates, when combined with vehicle motion, results in a decreased frequency of scan as illustrated in Figure 16.

5.3.3 Fidelity

Fidelity can be defined as "the accuracy of the representation when compared to the real world"[13]. The mean distance to target point was selected as the fidelity parameter, as it measures how accurately terrain in front of the vehicle was sampled. A Matlab simulation, using the same configuration detailed in Section 5.3, investigated the parameters affecting fidelity. Figure 17 plots the mean distance to the target point versus vehicle velocity and sample distance.

Given Figure 17 did not reveal any obvious trends, the data was further condensed into a 2-D bar graph. Figure 18 sums and averages the data along the Sample Distance axis, thus plotting mean distance to target versus the vehicle's velocity. From this Figure it is clear the mean distance to target is not dependent upon either the sample distance or velocity. The paramount factors affecting the system's fidelity are the encoder resolution[14] and the

[13]Taken from the SEDRIS online glossary.

[14]For 5000 pulses/rev encoder the mean distance to target is 0.0455m while a 1024 pulses/rev encoder increases

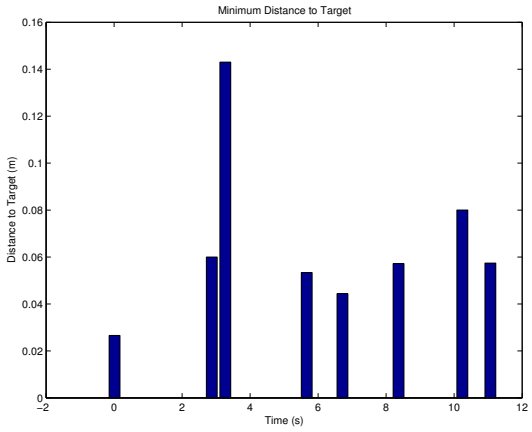

Figure 15: *Distance from Scan to Target Point*

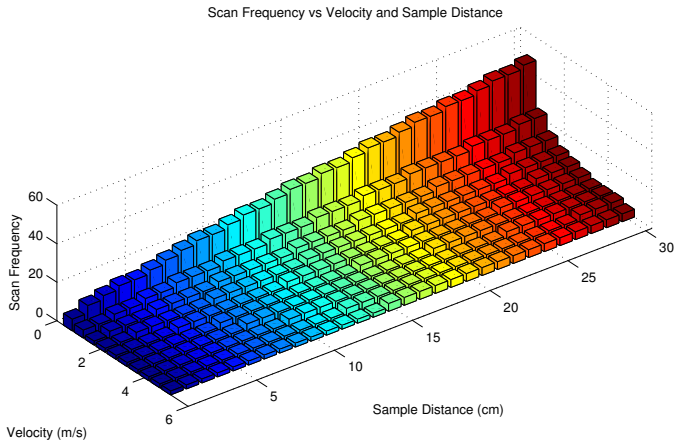

Figure 16: *Frequency of Scan vs Velocity and Sample Distance*

sweep period of the LRF; thus, a more accurate encoder and a shorter sweep period yields better resolution and fidelity.

5.4 Discussion

The vehicle's velocity and the size of the uniform sample distance do not affect the fidelity of a nodding LRF. Although an arbitrary sample distance can be defined, a smaller sample distance, yielding a finer resolution, requires a slower nodding rate. A slower nodding rate is undesirable since it produces a decreased frequency of scan. A high frequency of scan yields multiple terrain scans that produce better world representations. Field trials are required to determine the sample distances that are most suitable for varying terrain types.

this value to 0.2 m.

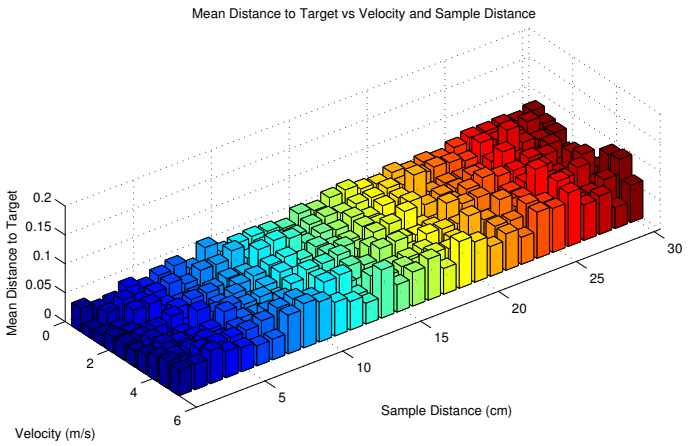

Figure 17: *Mean Scan to Target Point Distance*

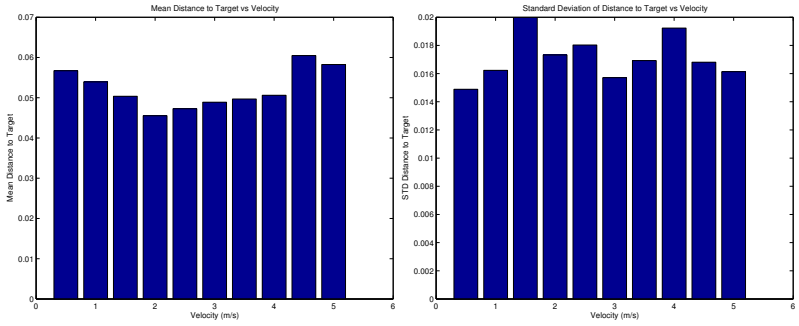

Figure 18: *Mean Scan to Target Point Distance by Velocity*

6. Characterizing the Nodding SICK Laser Performance

The nodding SICK laser's performance cannot be characterized without an understanding of the context in which it will be used. The nodding SICK laser mounts directly to the chassis of the vehicle. The chassis forms the basis for the vehicle's co-ordinate system from which a map co-ordinate system is derived. Before the laser's range data can be integrated into a world representation it must be transformed from the laser beam co-ordinate system into a map co-ordinate. These co-ordinate systems and transforms are described in the following sections.

6.1 Definition of Co-ordinate Systems

Figure 19 shows the co-ordinate systems. Roll occurs about the X axis, pitch is about the Y axis and yaw occurs about the Z axis.

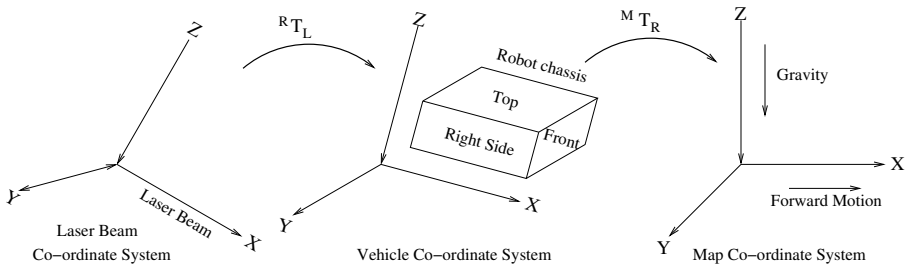

Figure 19: *Co-ordinate Systems and Transformations*

6.1.1 Map Co-ordinate System

The map co-ordinate system defines the X axis along the vector of forward motion; the Y axis is perpendicular to the X axis and the Z axis aligned with gravity.

6.1.2 Vehicle Co-ordinate System

The vehicle co-ordinate system is aligned with the chassis of the vehicle. The X axis lies along the front/back chord; the Y axis lies along the left/right chord and the Z axis is along the top/bottom chord. The nodding device aligns with this co-ordinate system.

6.1.3 Nodding Co-ordinate System

The nodding co-ordinate system is a plane that lies along angle of rotation about the Y axis that corresponds to the nodding angle of the device.

6.1.4 Laser Beam Co-ordinate System

The X axis for each laser range lies along the laser beam's projected line; thus, a point is always located at $(r, 0, 0)$ in this co-ordinate system.

6.2 Transformations

The SICK laser's range data is received relative to its own co-ordinate system. It is transformed to the vehicle co-ordinate system, and then to the map co-ordinate system as shown in Figure 19.

${}^{R}T_{L}$ gives the transformation between the laser and vehicle co-ordinate systems using the following measurements:

- Distance, d,

- SICK laser angle, ν, corresponding to a yaw motion,
- Nodding device angle, η, corresponding to a pitch motion.

${}^{M}T_{R}$ defines the transformation from vehicle co-ordinate system to the map co-ordinate system using the roll, pitch and yaw measurements from the inertial measurement unit (IMU):

- Roll, ϕ_{imu}
- Pitch, θ_{imu}
- Yaw, ψ_{imu}

The order of rotation [19] is specified as:

$$RPY(\phi,\theta,\psi) = Rot(x,\phi)Rot(y,\theta)Rot(z,\psi)$$

where:

$$Rot(x,\phi) = \begin{bmatrix} 1 & 0 & 0 & 0 \\ 0 & \cos\phi & -\sin\phi & 0 \\ 0 & \sin\phi & \cos\phi & 0 \\ 0 & 0 & 0 & 1 \end{bmatrix}$$

$$Rot(y,\theta) = \begin{bmatrix} \cos\theta & 0 & \sin\theta & 0 \\ 0 & 1 & 0 & 0 \\ -\sin\theta & 0 & \cos\theta & 0 \\ 0 & 0 & 0 & 1 \end{bmatrix}$$

$$Rot(z,\psi) = \begin{bmatrix} \cos\psi & -\sin\psi & 0 & 0 \\ \sin\psi & \cos\psi & 0 & 0 \\ 0 & 0 & 1 & 0 \\ 0 & 0 & 0 & 1 \end{bmatrix}$$

using the above rotations

$$RPY(\phi,\theta,\psi) = Rot(x,\phi) \begin{bmatrix} \cos\theta & 0 & \sin\theta & 0 \\ 0 & 1 & 0 & 0 \\ -\sin\theta & 0 & \cos\theta & 0 \\ 0 & 0 & 0 & 1 \end{bmatrix} \begin{bmatrix} \cos\psi & -\sin\psi & 0 & 0 \\ \sin\psi & \cos\psi & 0 & 0 \\ 0 & 0 & 1 & 0 \\ 0 & 0 & 0 & 1 \end{bmatrix}$$

$$RPY(\phi,\theta,\psi) = \begin{bmatrix} 1 & 0 & 0 & 0 \\ 0 & \cos\phi & -\sin\phi & 0 \\ 0 & \sin\phi & \cos\phi & 0 \\ 0 & 0 & 0 & 1 \end{bmatrix} \begin{bmatrix} \cos\theta\cos\psi & -\cos\theta\sin\psi & \sin\theta & 0 \\ \sin\psi & \cos\psi & 0 & 0 \\ -\sin\theta\cos\psi & \sin\theta\sin\psi & \cos\theta & 0 \\ 0 & 0 & 0 & 1 \end{bmatrix}$$

$$RPY(\phi,\theta,\psi) = \begin{bmatrix} \cos\theta\cos\psi & -\cos\theta\sin\psi & \sin\theta & 0 \\ \cos\phi\sin\psi+\sin\phi\sin\theta\cos\psi & \cos\phi\cos\psi-\sin\phi\sin\theta\sin\psi & -\sin\phi\cos\theta & 0 \\ \sin\phi\sin\psi-\cos\phi\sin\theta\cos\psi & \sin\phi\cos\psi+\cos\phi\sin\theta\sin\psi & \cos\phi\cos\theta & 0 \\ 0 & 0 & 0 & 1 \end{bmatrix}$$

The first step in the transformation from the laser beam[15] to the vehicle co-ordinate system is to determine the (x,y) co-ordinates relative to nodding co-ordinate system[16]:

$$p_i = d_i\left(\cos\psi_i\hat{i} - \sin\psi_i\hat{j}\right)$$

The transformation to the vehicle co-ordinate[17] system from the map co-ordinate system is given by:

$$p_i = (x_i\cos\theta_i)\hat{i} + y\hat{j} + (x_i\sin\theta_i)\hat{k}$$

These transformations convert the laser's range measurement into 3-D data set in the map co-ordinate; therefore, a terrain map can directly use this data.

The vehicle to world co-ordinate system must use the full rotation matrix.

6.3 Factors Influencing the Measurement Accuracy

A world representation requires 3-D data in the map co-ordinate system. The accuracy of the 3-D data is affected by all measurements required to acquire and transform the laser range data. Measurement errors are associated with the following:

1. Pose estimation, consisting of:
   (a) Position estimation of the vehicle's X , Y and Z co-ordinates,
   (b) Orientation estimation of the roll, pitch and yaw of the vehicle.

[15] Defined as $(r,0,0)$.
[16] Note: This co-ordinate system has only (*x*,*y*) values, and no *z* component.
[17] This co-ordinate system has only the pitch, θ, as a component of the transformation.

2. Nodding LRF

   (a) SICK laser range measurement,

   (b) Orientation of laser beam in terms of pitch and yaw.

The following sections provide details on the sources of error.

6.3.1 SICK Laser Range Measurement Error

The SICK laser distance measurement is subject to systematic errors that results in an accuracy of ± 4 cm over its operating range.

6.3.2 Position Error

The position error is comprised of three components, corresponding to the X , Y and Z axes. This error encompasses a sphere around the true position of the vehicle. Using the NovaTel DL-4-RT2 DGPS receiver, the position error is ± 3 cm along each axis.

6.3.3 Orientation Error

Orientation is affected by the following factors:

- The encoder resolution of the nodding device is 0.072 degrees,
- The positioning of the SICK laser beam has a resolution of 1 ± 0.1 degrees.
- An on-board IMU determines the vehicle's roll, pitch and yaw. The IMU's accuracy varies between devices, with the Microstrain 3DM-GX1 and 3DM-G IMUs having an accuracy of ± 2 and ± 5 degrees respectively.

The basic geometry of a right angle triangle, with a long hypotenuse, reveals a small change in angle will significantly change the magnitude of the opposite leg. This geometry applies to the nodding LRF configuration, as shown in Figure 20.

In Figure 20 $\Delta\varepsilon$ is the error in pitch orientation, r is range measured by the LRF and Δs is the error in position. For small angles of rotation, less than 10 to 15 degrees, the position error can approximated using the small angle assumption:

$$\Delta s \simeq r\Delta\varepsilon$$

Building upon the 2-D case, Figure 21 shows the geometry for the position error in 3 dimensions. To simplify the positional error derivation, the

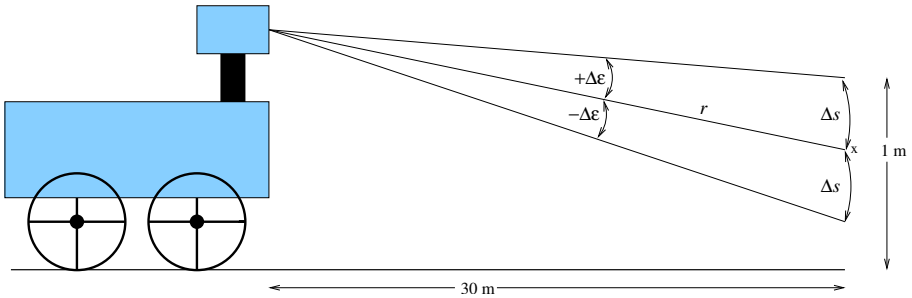

Figure 20: *Orientation Error in 2-D*

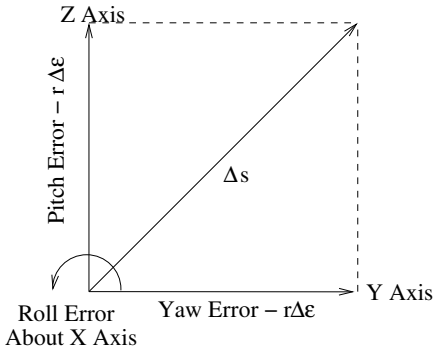

Figure 21: *Orientation Error in 3-D*

orientation error is assumed to have symmetric properties where $\Delta\phi = \Delta\theta = \Delta\psi = \Delta\varepsilon$. The error Δs is the vector resulting from the pitch and yaw errors. The roll error occurs about the X axis does not contribute to the magnitude of the error, but rotates the arc, Δs, in 3-D space. Using the small angle approximation, the orientation error in three dimensions is given by:

$$\Delta s \simeq \sqrt{(r\Delta\varepsilon)^2 + (r\Delta\varepsilon)^2} = \sqrt{2(r\Delta\varepsilon)^2}$$

Figure 22 shows the magnitude of the 3-D error versus the LRF distance and the orientation error. As can be seen in the Figure 22, the measurement error increases with both the error in the orientation estimate and the distance measured by the LRF.

The errors, for selected distances from Figure 22, are also tabulated in Table 1.

6.4 Discussion

These investigations show the vehicle's roll, pitch and yaw are the dominant error source. These errors are at least an order of magnitude more significant than other

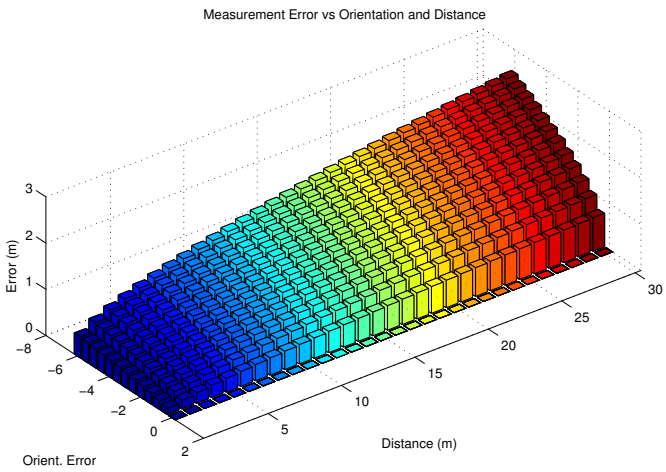

Figure 22: *Measurement Error vs. Orientation and Distance*

	Angle					
Distance	1.0	2.0	3.0	4.0	5.0	6.0
1	0.19	0.26	0.32	0.37	0.41	0.45
5	0.42	0.59	0.72	0.84	0.93	1.02
10	0.59	0.84	1.02	1.18	1.32	1.45
15	0.72	1.02	1.25	1.45	1.62	1.77
20	0.84	1.18	1.45	1.67	1.87	2.05
25	0.93	1.32	1.62	1.87	2.10	2.28
30	1.02	1.45	1.77	2.05	2.29	2.51

Table 1: *Measurement Error vs. Orientation and Distance*

source of errors. Table 1 shows the absolute magnitude of these errors are comparable to the physical dimensions of many vehicles and they can not be safely ignored.

7. Implementation on the Raptor UGV

7.1 Introduction

The ALS project, using the Miro architecture [20, 21, 22], implemented nodding SICK lasers on the Raptor UGV. Figure 23 shows the Raptor with both front and rear mounted nodding SICK lasers. Acting as the *eyes* of the vehicle, the front nodding SICK laser is the paramount sensing device on the Raptor UGV. The laser's 3D data is the primary data source for generating the terrain maps [7] used in obstacle/hazard detection and avoidance.

Figure 23: *Raptor UGV with Nodding SICK Laser*

7.2 Implementation under Miro

7.2.1 Configuration

As described in Section 3., the nodding SICK laser downloads an embedded, executable application that controls the nodding device's motor and the SICK laser. The nodding laser's boot code uses *bootp* to search for a *dhcpd* server that responds to its MAC address and when found, retrieves an initial IP address. It then uses *tftp* to download the executable application, after which it proceeds to boot the application. At this point the application assigns the nodding laser an internally coded IP address. The following parameters define the current nodding laser configuration:

- Dhcpd server address as defined in dhcpd.conf: 10.10.10.30.
- MAC address range of the nodding laser device: 06:53:49:4C:00:01 - 06:53:49:4C:00:07
- Name of the executable applications, including the absolute path: /bootfiles/m68360/silsick.exe, as defined in dhcpd.conf.
- Hard coded IP address of executable application: 10.10.10.230.

7.2.2 Driver

The nodding laser's Miro driver follows the Publish Server and Reactor design pattern [23], as show in Figure 24. Via TCP/IP communications over an ethernet link, this driver controls and acquires range data from the nodding SICK laser, and processes it into a CORBA object. This object is then placed

on the CORBA eventChannel for consumption by clients. The CORBA object may also be accessed via a polled interface.

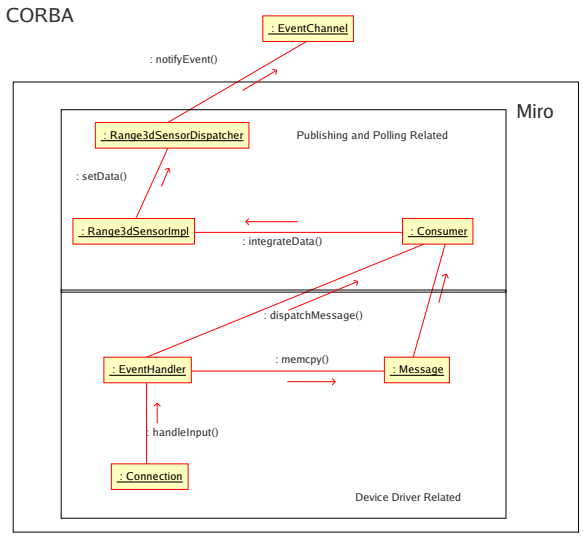

Figure 24: *Nodding Laser Publish Server and Reactor Design Pattern*

A summary of the main classes and their function is given below:

1. **Connection -** The *Connection* class is responsible for managing the TCP/IP socket connection to the nodding Laser. This includes setting up the connection, sending commands to the device and the receipt of range data. It is important to note that the *Connection* does not process data from the nodding laser, but rather signals the *EventHandler* that new data has arrived.

2. **EventHandler -** The *EventHandler* asynchronously reads raw range data from the *Connection* using the *handle_input* callback method. The callback method synchronizes to the new datagram's start, reads the entire datagram into a buffer, and copies the buffer to the *Message* class. Once the buffer has been copied, the *dispatchMessage* method is called signalling the *Consumer* that a new packet of information is available.

3. **Message -** The *Message* class contains a buffer for holding a range datagram and provides methods for retrieving buffered data.

4. **Consumer -** The *Consumer* class processes range data through the event driven *handle_message* method. Each time the *EventHandler* calls *dispatchMessage* the *Consumer* reads the data from the *Message* and populates the various fields of a *Range3d<types>EventIDL* CORBA object. This generic description of 3-D data is then passed to the *Range3dSensorImpl* class via its *integrateData* method.

5. **Range3dSensorImpl** - The *integrateData* method, in the *Range3dSensorImpl* class, copies the nodding laser data into a locally allocated *Range3d<types>EventIDL* CORBA object. Using this local structure the *NoddingLaser's* server implementation responds to polling requests. Before returning, *integrateData* passes the *Range3d<types>EventIDL* CORBA object to the *setData* method.

6. **Range3dSensorDispatcher** - The *Range3dSensorDispatcher* takes the *Range3d<type>EventIDL* CORBA object and publishes the CORBA object on the *EventChannel* via the *dispatch* method.

7.2.3 CORBA Objects

The nodding laser driver implements two of CORBA objects, following the *Range3d<types>EventIDL* naming scheme, that facilitate the distribution of laser 3-D data:

- *Range3dSeqEventIDL*: Generic 3-D range data derived from C++ sequences.
- *Range3dLaserEventIDL*: A fixed length array of 3-D range data optimized for the SICK laser.

Shown below is the CORBA IDL code to implement the generic 3-D CORBA object.

```
struct Range3dSeqEventIDL
{
  //! The time the scan was acquired.
  TimeIDL time;
  //! Angle of the nodding laser in radians
  double nodangle;
  //! The full scan of all sensor groups.
  RangeScanIDL range3d;
};
```

The CORBA IDL code, implementing the SICK laser specific code, is shown in the following code listing.

```
//! An array of 3d point groups.
typedef double Range3dLaserIDL[LASER_NUM][PLANES_NUM];
struct Range3dLaserEventIDL
{
  //! The time the scan was acquired.
```

```
  TimeIDL time;
  //! Angle of the nodding laser in radians
  double nodangle;
  /* ID of the Laser */
  long laser_ID;
  //! The data, X, Y, Z and the range
  Range3dLaserIDL range3d;
};
```

The sequenced based CORBA object sacrifices speed for improved data abstraction, and the fixed length array based CORBA object optimizes performance.

7.3 Debugging and Visualization Components

The *QtRange3dSensor* tool, shown in Figure 25, presents a visual display of generic range and 3-D data. The interface on the left side shows the raw SICK laser range data, and the interface on the right shows the data transformed into its Z elevation at each Y co-ordinate location[18]. These visual interfaces proved invaluable in debugging, calibrating and understanding the operation of the nodding SICK laser.

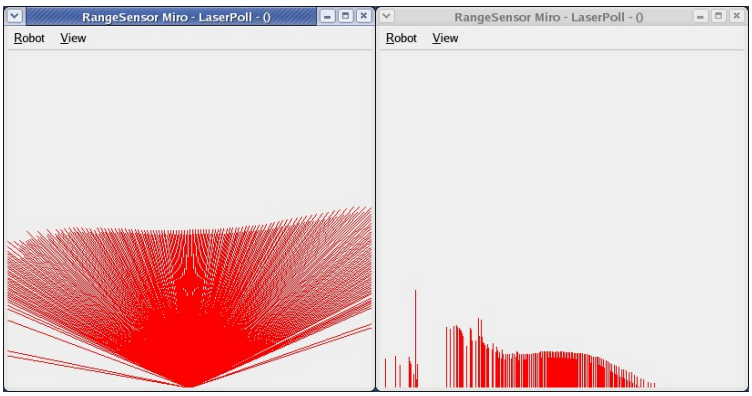

Figure 25: QtRange3dSensor *Visualization Interface*

Table 2 shows the debugging printout from the *Sensor3dGet*/*Sensor3dStream*[19] debugging components. These debugging tools print the raw range and the (x,y,z) components.

[18]The X co-ordinate is not displayed in the 2-D view.
[19]The *Sensor3dGet* component implements polling, while the *Sensor3dStream* responds to events.

Sample	Range (mm)	X (mm)	Y mm	Z (mm)
1	35840	14478	32724	357
2	35410	14584	32204	372
3	34360	14422	31123	350
4	33940	14511	30615	372
5	33610	14632	30189	379
6	33360	14783	29835	400
7	Invalid	-	-	-

Table 2: *Debug Range and 3-D Data*

7.4 Calibration

As can be seen in Figure 23 the SICK laser mounts on the Raptor's inclined roof. Both the roof inclination and the mounting height are unknowns. The calibration process solves these unknowns using a two stage process.

7.4.1 Laser Mount Angle

When the Raptor vehicle sits on a flat floor, such as a cement pad, the nodding laser should return a consistent Z elevation. The uncalibrated nodding SICK laser does not return a consistent Z co-ordinate due to the Raptor's inclined roof. To determine the laser's mounting angle:

1. The estimated roof inclination was added to the *ModelServer* geometry database [24] as a homogeneous transform,
2. The Z elevation was monitored using the *Sensor3dGet*/*Sensor3dStream* component,
3. If the Z elevation did not supply a consistent value, the estimated roof inclination was modified and the *ModelServer* geometry database was updated,
4. Steps 2 and 3 were repeated until the Sensor3dGet*Sensor3dGet*/*Sensor3dStream* printout registered a consistent Z elevation.

Using the above process the laser mount angle converged on a value of 11.33 degrees.

7.4.2 Laser Mount Height

Once the laser mount angle has been determined the laser mount height is given by the Z elevation printed by *Sensor3dGet*/*Sensor3dStream* component.

For the Raptor vehicle the Z elevation was 1.64 m and this value was registered with the *ModelServer*.

7.5 Performance

7.5.1 Configuration

The configuration aspects of the nodding SICK laser were onerous. The current configuration demands a 10.10.10.x subnet, which does not coincide with the subnet provided by the on-board SpeedLan mesh network router. Thus, the Raptor's quad Pentium server, configured as a router, was required to bridge internal ethernet ports. This extra router required additional configuration/setup, and proved problematic for CORBA Naming Services and component bindings. By default CORBA binds to the first available ethernet interface, which in this case must be the SpeedLan mesh router. But ethernet interfaces are numbered by their configuration order; thus, the ethernet interface corresponding to the SpeedLan router must always be configured first.

7.5.2 Scanning

The nodding SICK laser driver implemented only a fixed nodding rate and a static field of view. The ALS project's demonstration deadline precluded the implementation of adaptive nodding rates and fields of view, as well as the uniform sample distance profile. Even though the nodding SICK laser implementation was sub-optimal, its performance was more than adequate. The nodding mechanism, allowing multiple scans over the same terrain, performed very well. Multiple scans result in a terrain map with higher data densities, more reliable statistics, and maps that better represent the world.

Table 3 gives the computational resources consumed for both types of CORBA *Range3d* objects and shows the sequenced based CORBA object consumes significantly more the CPU resources. Given the ALS project was DRDC's first demonstration of a complex UGV a conservative approach was taken that used the fixed length array, *Range3dLaserEventIDL,* CORBA object.

CORBA Object	CPU %	Memory %
Range3dSeqEventIDL	3.3	4.5
Range3dLaserEventIDL	2.0	4.5

Table 3: *Computational Resources Consumed*

Originally the Raptor vehicle featured a single forward looking, nodding laser, but under this configuration the terrain maps suffered from a lack of data density. With minimal software modifications, a second forward looking,

nodding laser was added, which doubled the data densities received by the terrain map.

Although the nodding SICK laser performed admirably it was not without flaws. The current nodding mechanism does not use a gear reduction; thus, the stepper motor must operate through a range where rotational rate fluctuates. Given the nodding mechanism uses a feedback encoder these oscillations do not cause problems, but this idiosyncrasy must be address for the uniform sample profile implementation. The lack of a gear reduction may also contribute to overheating problems, which occasionally caused the device to fail. Finally, direct sunlight blinds the SICK laser and places it into a failure mode. The current Miro driver does not detect this failure and hence does not reset the laser and restart scanning. Thus, while the laser continues nodding it does not provide range data.

8. Conclusions

This report investigated the nodding LRF, in the context of supplying 3-D data to terrain maps. A literature search revealed that historically LRFs have been used as single scan devices where the terrain in front of the vehicle is sampled only once. This single sample approach suffers from a number of deficiencies including occlusions, mixed pixels and sunlight blinding. This research implemented a nodding SICK laser as a means to alleviates the issues associated with the single sample approach, and determined that multiple terrain scans yielded high data densities, thus more accurate world representations.

This report researched the error sources limiting the accuracy of a vehicle mounted, nodding LRF. It was determined the errors in roll, pitch and yaw are at least an order of magnitude more significant than any other error source. This error, when applied to the range returned by the LRF, can be viewed as a sphere that encircles true position of the point's co-ordinates. This sphere can be interpreted as the statistical variance associated with the point.

A variety of nodding profiles can be implemented by a nodding LRF. Geometry effects were investigated and the uniform sample distance nodding profile was determined to be the most attractive implementation. This report presented theoretical research and simulations that detailed the advantages of uniform sampling. The uniform sample profile maintains the desired sample distance over all vehicle velocities; thus, providing 3-D data at a predefined and nearly constant density. The uniform sample distance was the preferred nodding profile, but due to time constraints the ALS demonstration implemented only the constant angular rate profile.

The theoretical effects of vehicular motion were also investigated. Simulations revealed the sample distance and scan frequency are opposing factors. A smaller sample distance requires a slower rotational rate, which yields a decreased frequency of scan.

Selecting a suitable sample distance will require experimentation and field trials.

DRDC developed a Miro driver for the nodding SICK laser. This driver transforms the raw laser range data into 3-D data before publishing it as a CORBA 3-D range event. This 3-D data was the primary data source for the Raptor's terrain mapping capability, and thus played a critical role in enabling intelligent obstacle/hazard avoidance behaviors.

The current nodding SICK laser configuration proved sufficient for the ALS demonstration; future work will extend the Miro driver. A key extension will be the support for adaptive nodding rates and the capability to create the uniform sample distance profile. The laser also suffered from occasional overheating, oscillations and sunlight blinding. These issues will be addressed with hardware modifications and driver enhancements.

References

1. Herbert, M. and Krotkov, E. (1993). Local Perception for Mobile Robot Navigation in Natural Terrain: Two Approaches. In *Workshop on Computer Vision for Space Applications*, pp. 24–31.

2. Kweon, S. and Kanade, T. (1992). High-Resolution Terrain Map from Multiple Sensor Data. *IEEE Transactions on Pattern Analysis and Machine Vision, 14*(2), 278–292.

3. Bellutta, P., Manduchi, R., Matthies, L., Owens, K., and Rankin, A. (2000). Terrain Perception for DEMO III. In *Proceedings of the 2000 Intelligent Vehicles Conference*.

4. Goldberg, S., Maimone, M., and Matthies, L. (2002). Stereo Vision and Rover Navigation Software for Planetary Exploration. *IEEE Aerospace Conference Proceedings*.

5. Lacroix, S., Mallet, A., and Bonnafous, D. (2000). Autonomous Rover Navigation on Unknown Terrains Demonstrations in the Space Museum "Cite de l'Espace" at Toulouse Automation, Albuquerque, USA, 1997. In *7th International Symp. on Experimental Robotics*, pp. 669–683. Honolulu, HI.

6. Kelly, A. (1997). Intelligent Unmanned Ground Vehicles: Autonomous Navigation Research at Carnegie Mellon, Ch. RANGER: Feedforward Control Approach to Autonomous Navigation, pp. 105–144. Kluwer Academic Publishers.

7. Broten, G., Giesbrecht, J., and Monckton, S. (2005). World Representation Using Terrain Maps. (DRDC Suffield TR 2005-248). Defence R&D Canada – Suffield. Medicine Hat, Alberta.

8. Herbert, M. (2000). Active and Passive Range Sensing for Robotics. In *IEEE International Conference on Robotics and Automation*, pp. 102–110. IEEE. San Franscisco, CA.

9. S. Kweon, R. Hoffman and Krotkov, E. (1991). Experimental Characterization of the Perceptron Laser Rangefinder. (Technical Report CMU-RI-TR-91-1). Carnegie Mellon University. Pittsburg, Pennsylvania 15213.

10. Herbert, M. and Krotkov, E. (1992). 3-D Measurements from Imaging Laser Radars: How Good Are They?. *International Journal of Image and Vision Computing*, *10*(3), 170–178.

11. Hoffman, R. and Krotkov, E. (1991). Perception of Rugged Terrain for a Walking Robot: True Confessions and New Directions. In *IEEE/RSJ International Workshop on Intelligent Robots and Systems*, pp. 1505–1510. IROS.

12. Ye, C. and Borenstien, J. (2002). Characterization of a 2-D Laser Scanner for Mobile Robot Ostacle Negoation. In *Proceddings of the 2002 IEEE International Conference on Robotics and Automation*, pp. 2512–2518. Washington, DC, USA.

13. C. Thorpe, T. Kanade, M. Herbert and Shafer, S. (1988). Vision and Navigation for the Carnegie-Mellon Navlab. *IEEE Transactions on Pattern Analysis and Machine Intelligence, 10*(3), 362–373.

14. Herbert, M., Caillas, C., Krotkov, E., Kweon, I., and Kanade, T. (1989). Terrain Mapping for a Roving Planetary Explorer. In *Proceedings of the IEEE International Conference on Robotics and Automation*, pp. 997–100.

15. M. Herbert, T. Kanada and Kweon, I. (1988). 3-D Vision Techniques for Autonomous Vehicles. (Technical Report CMU-RI-TR-88-12). Carnegie Mellon University. Pittsburg, Pennsylvania, 15213.

16. Henriksen, L. and Krotkov, E. (1997). Natural Terrain Hazard Detection with a Laser Rangefinder. In *Proceedings IEEE International Conference On Robotics and Automation*, pp. 968–973. Albuquerque, New Mexico.

17. Apostolopoulos, D. S. (2000). Technology and field demonstration of robotic search for Antarctic meteorites. *International Journal of Robotics Research*, *19*(11), 1015–1032.

18. Ye, C. and Borenstien, J. (2003). A New Terrain Mapping Method for Mobile Robot Obstacle Negotiation.. In *Proceedings of the UGV Technology Conference at the 2003 SPIE AeroSense Symposium*, Orlando, FL.

19. Paul, R.P. (1981). Robot Manipulators-Mathematics, Programming and Control, MIT Press.

20. Broten, G., Monckton, S., Giesbrecht, J., Verret, S., Collier, J., and Digney, B. (2004). Towards Distributed Intelligence. (DRDC Suffield TR 2004-287). Defence R&D Canada – Suffield. Medicine Hat, Alberta.

21. Broten, G., Monckton, S., Giesbrecht, J., and Collier, J. (2006). Software Sysetms for Robotics, An Applied Research Perspective. *International Journal of Advanced Robotic Systems*.

22. Broten, G. and Monckton, S. (2005). Frameworks and Middleware for Unmanned Ground Vehicles. In *Proceedings of SPIE Symposium on Mobile Robots*.

23. Broten, G., Moncton, S., Giesbrecht, J., and Collier, J. (2006). Software Engineering for Experimental Robotics, Ch. UxV Software Systems, An Applied Research Perspective. Springer Tracts in Advanced Robotics.

24. Monckton S., Broten G., Vincent I. (2006). A Prototype Vehicle Geometry Server: Design and development of the ModelServer CORBA Service. (DRDC Suffield TR 2005-240). Defence R&D Canada – Suffield. Medicine Hat, Alberta.

DOCUMENT CONTROL DATA

(Security classification of title, body of abstract and indexing annotation must be entered when document is classified)

1. ORIGINATOR (the name and address of the organization preparing the document. Organizations for whom the document was prepared, e.g. Centre sponsoring a contractor's report, or tasking agency, are entered in section 8.)

Defence R&D Canada – Suffield
PO Box 4000, Medicine Hat, AB, Canada T1A 8K6

2. SECURITY CLASSIFICATION (overall security classification of the document including special warning terms if applicable).

UNCLASSIFIED

3. TITLE (the complete document title as indicated on the title page. Its classification should be indicated by the appropriate abbreviation (S,C,R or U) in parentheses after the title).

The Characterization of an Inexpensive Nodding Laser (U)

4. AUTHORS (Last name, first name, middle initial. If military, show rank, e.g. Doe, Maj. John E.)

G.S. Broten and J.A. Collier

5. DATE OF PUBLICATION (month and year of publication of document)

December 2005

6a. NO. OF PAGES (total containing information. Include Annexes, Appendices, etc).

44

6b. NO. OF REFS (total cited in document)

24

7. DESCRIPTIVE NOTES (the category of the document, e.g. technical report, technical note or memorandum. If appropriate, enter the type of report, e.g. interim, progress, summary, annual or final. Give the inclusive dates when a specific reporting period is covered).

Technical Report

8. SPONSORING ACTIVITY (the name of the department project office or laboratory sponsoring the research and development. Include address).

Defence R&D Canada – Suffield
PO Box 4000, Medicine Hat, AB, Canada T1A 8K6

9a. PROJECT OR GRANT NO. (if appropriate, the applicable research and development project or grant number under which the document was written. Specify whether project or grant).

9b. CONTRACT NO. (if appropriate, the applicable number under which the document was written).

10a. ORIGINATOR'S DOCUMENT NUMBER (the official document number by which the document is identified by the originating activity. This number must be unique.)

DRDC Suffield TR 2005-232

10b. OTHER DOCUMENT NOs. (Any other numbers which may be assigned this document either by the originator or by the sponsor.)

11. DOCUMENT AVAILABILITY (any limitations on further dissemination of the document, other than those imposed by security classification)

(X) Unlimited distribution
( ) Defence departments and defence contractors; further distribution only as approved
( ) Defence departments and Canadian defence contractors; further distribution only as approved
( ) Government departments and agencies; further distribution only as approved
( ) Defence departments; further distribution only as approved
( ) Other (please specify):

12. DOCUMENT ANNOUNCEMENT (any limitation to the bibliographic announcement of this document. This will normally correspond to the Document Availability (11). However, where further distribution beyond the audience specified in (11) is possible, a wider announcement audience may be selected).

Unlimited

13. ABSTRACT (a brief and factual summary of the document. It may also appear elsewhere in the body of the document itself. It is highly desirable that the abstract of classified documents be unclassified. Each paragraph of the abstract shall begin with an indication of the security classification of the information in the paragraph (unless the document itself is unclassified) represented as (S), (C), (R), or (U). It is not necessary to include here abstracts in both official languages unless the text is bilingual).

The accuracy and reliability of laser rangefinders make them a ubiquitous sensing device employed on many unmanned ground vehicles. Expensive, high performance 3-D laser rangefinders enjoy limited acceptance, whereas static mounts are the preferred configuration for low cost 2-D laser rangefinders. This paper investigates and characterizes the factors affecting the nodding 2-D laser's performance. This research determined errors in measuring the vehicle's roll, pitch and yaw have the greatest impact on measurement accuracy. Analysis and simulations revealed that adaptive nodding rates offered unique advantages, especially when used with a terrain map world representation. The nodding mechanism also allows for the acquisition of multiple range data sets over the same terrain patch. These multiple data sets alleviate some of the problems traditionally associated with laser rangefinders, but they place more stringent requirements on the vehicle's pose accuracy. DRDC, in conjunction with Scientific Instrumentation Ltd., developed an inexpensive nodding SICK laser device and this device's 3-D data was an essential contributor to the successful Autonomous Land Systems demonstration.

14. KEYWORDS, DESCRIPTORS or IDENTIFIERS (technically meaningful terms or short phrases that characterize a document and could be helpful in cataloguing the document. They should be selected so that no security classification is required. Identifiers, such as equipment model designation, trade name, military project code name, geographic location may also be included. If possible keywords should be selected from a published thesaurus. e.g. Thesaurus of Engineering and Scientific Terms (TEST) and that thesaurus-identified. If it not possible to select indexing terms which are Unclassified, the classification of each should be indicated as with the title).

sensing, perception, rangefinders, lasers